

Measurement of the Rayleigh surface-phonon dispersion curve for NaCl(001) from high-resolution He time-of-flight spectroscopy and from kinematical focusing angles

G. Benedek,* G. Brusdeylins, R. Bruce Doak,[†] J. G. Skofronick,[‡] and J. Peter Toennies

Max-Planck-Institut für Strömungsforschung, Böttlingerstrasse 4-8, D-3400 Göttingen, Federal Republic of Germany

(Received 18 April 1983)

Angular distributions and time-of-flight spectra have been measured for the collisions of 20-meV He atoms with a NaCl(001) surface in the $\langle 100 \rangle$ direction. Structures in the angular distribution and in the time-of-flight spectra due to elastic and inelastic scattering are measured and used to extract (1) a corrugation parameter of the rigid-atom surface potential $\zeta_0 = 0.34 \text{ \AA}$, (2) three bound-state energies of the He-surface potential, and (3) a surface-phonon Rayleigh dispersion curve out to the edge of the Brillouin zone. Furthermore, we were able to demonstrate that by rotating the crystal about the surface normal it is possible to unambiguously identify kinematical focusing features in the angular distributions. These features were then used to determine a surface-phonon dispersion curve in good agreement with that obtained from the time-of-flight experiments.

I. INTRODUCTION

The ability to definitively measure both elastic and inelastic collision processes of He atoms from single alkali halide crystal surfaces with high resolution has opened up new experimental and theoretical possibilities for surface studies of these systems.¹⁻⁹ The basic procedure for inelastic experiments uses the time-of-flight (TOF) method in which a pulsed nearly monoenergetic He beam of about 20 meV is directed upon a crystal surface and the scattered beam is detected as a function of time.¹⁻⁵ An observed gain in energy by the scattered He beam is produced by surface-phonon annihilation events while a loss in energy results from creation events. Since mostly single-phonon collisions are involved the changes in energy show up as well-resolved peaks in the TOF spectra and yield directly via the conservation equations the surface-phonon dispersion curve for the crystal.^{2,3}

Four crystals (LiF, NaF, KCl, MgO) have been previously studied^{1-5,10} in this laboratory. Surface-phonon dispersion curves have been measured and bound-state energy levels of the He-surface interaction potential have either been found or confirmed. The process of phonon-assisted selective desorption involving elastic selective adsorption of the atoms on the surface followed by ejection via an inelastic collision with a surface phonon⁷ has been clearly elucidated. In addition, a number of other processes involving phonons and transitions into and out of bound states as well as between bound states have been observed.¹⁰⁻¹²

The present study of NaCl was motivated by the observation that in the case of LiF $\langle 100 \rangle$ the measured Rayleigh-surface dispersion curve was found to lie below the theoretical curve for $Q \gtrsim 1 \text{ \AA}^{-1}$ and at the zone boundary $Q = 1.6 \text{ \AA}^{-1}$ the difference between observed and calculated frequencies amounted to about 14%.^{1,3} A similar discrepancy was not observed in the case of NaF or KCl.²⁻⁵ The current explanation of the discrepancy is that it is due to two opposing effects¹³: A geometrical relaxation of the distance between lattice planes near the surface which is expected to occur (but not included in the

calculation) will lead to an increase in frequency. On the other hand, the change in the electronic structure near the surface is expected to increase the polarizability of the F ions at the surface and decrease the frequency. According to the calculations of Benedek, Miglio, and co-workers^{14,15} the latter effect alone can explain the discrepancy in LiF, whereas in NaF and KCl, where the halogen ion is at rest in the zone-boundary Rayleigh mode, such a mechanism is ineffective. On the other hand, in NaCl, where the relative masses and sizes of the ions are more comparable to those of LiF, and the halogen ion is vibrating at the zone boundary, we might expect an increase in polarizability and charge transfer to be an important effect. The surface-phonon dispersion curves for the unrelaxed surface have been calculated by Chen, de Wette, and Alldredge¹⁶ using the slab method and by Benedek¹⁷ and Benedek and Miglio¹⁴ using the Green's-function method. These calculations are in reasonable agreement except near the zone boundary, where the differences are of the order of 7%. The good agreement found in this work between both these uncorrected theories and experiment suggests that either the polarizability change effect is weak in NaCl, or the polarizability and elastic relaxation mechanisms compensate each other.

Surprisingly few scattering experiments have been performed on NaCl single crystals. Some previous experimental work on elastic scattering was done by Bledsoe and Fisher.¹⁸ As recently pointed out by Rieder their results may have been affected by the poor background pressure in their apparatus.¹⁹ For this reason they also had to maintain their crystal at room temperature which increased the inelastic background. Our work, which was also mostly at room temperature, indicated no unusually large phonon contribution, however. Their data were evaluated by Garcia, Armand, and Lapujoulade to determine a surface corrugation parameter.²⁰ Bledsoe also reports angular scans which reveal poorly resolved selective adsorption minima.²¹ From these he was able to determine one bound state of the He-NaCl potential. The scattering of H atoms from NaCl has been recently studied by Iannotta and Valbusa²² and by Bätz, Hoinkes, and

Wilsch,²³ and bound-state energies were determined.

Section II is a short experimental section. In Sec. III the TOF spectra are presented and interpreted in terms of surface-phonon dispersion relations. Next the angular distributions are analyzed. From the diffraction intensities the corrugation of the hard corrugated surface is determined. Structures between the diffraction peaks are analyzed in terms of selective desorption and give information on the bound states. Other structures are attributed to kinematic focusing (KF) and have been used to provide an independent confirmation of the phonon dispersion curves. The results are discussed in Sec. IV.

II. EXPERIMENTAL

The apparatus is the same as that used previously and described in detail elsewhere,^{2,3,7} thus only a brief description will be given. A high-pressure (200-atm) nozzle source is operated near 80 K to produce a He beam of about 20-meV energy with a velocity full width at half maximum (FWHM) $\Delta v/v \simeq 9 \times 10^{-3}$.^{24,25} This beam is collimated to a FWHM of approximately 0.3° , chopped at 300 Hz into pulses of $4\text{-}\mu\text{s}$ duration, and is scattered from the surface of a NaCl crystal held by a manipulator. The scattered beam passes through several differential pumping stages before being detected by a magnetic mass-spectrometer detector permanently positioned at an angle of 90° to the incident beam. A multichannel analyzer with $6.9\text{-}\mu\text{s}$ channel resolution is used in the TOF mode to successively store the scattered pulsed signal. By measuring over a period of typically 3–8 h a good signal-to-noise ratio is achieved. The path length from the chopper to the detector is 206.1 cm while that from the target to the detector is 115.4 cm.

The crystals of NaCl were obtained from Firma Korth, Kiel.²⁶ The samples ($10 \times 7 \times 2 \text{ mm}^3$) were cleaved in air, mounted immediately, and evacuated. The crystal and target chamber were then baked at temperatures near 350 K for approximately 10 h. This produced experimental vacuum conditions in the scattering chamber in the low 10^{-9} -Torr range. The crystal was then given a much more thorough bakeout (750 K for 6–12 h) after which measurements were begun. During this later bakeout the signal-to-noise ratio and structure in the angular scans continued to improve, but eventually stabilized. The appearance of repeatable angular scans and TOF spectra were taken as a sign that the surface was clean.^{2,3,27} The crystal was rebaked at intervals for several days as was also done previously for LiF. Two samples were used. The first was cleaved and mounted and preliminary results were obtained. It produced good TOF spectra, but due to an alignment problem it was removed. The second sample reproduced the TOF spectra of the first sample and it was used for most of the work reported in this paper. The beam intensity, the detector sensitivity, and the measuring time for the spectra were regularly monitored so that the spectra taken on different days could be normalized and compared in amplitude as well as in time.

The target temperature was measured with a thermocouple attached to one of the clips which holds the crystal to the manipulator. Most of the work presented herein was done with the crystal at 298 K; however, some were measured at approximately 220 K.

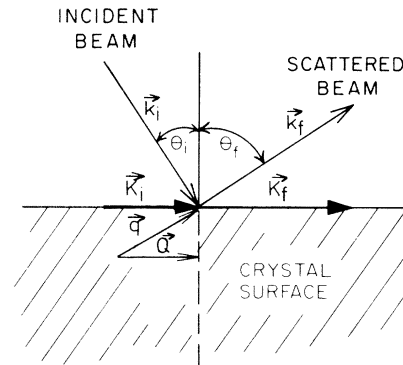


FIG. 1. Relationship between the incident and scattered wave represented by wave vectors \vec{k}_i and \vec{k}_f , respectively. A bulk phonon with a surface-momentum component \vec{Q} is also shown.

The TOF spectra were measured for different incident angles θ_i (θ_i is equal to the angle between crystal normal and incident beam) as is shown in Fig. 1. Note that because of the fixed angle between the incident and outgoing beam the final angle θ_f is fixed by $\theta_f = 90 - \theta_i$ in all experiments. The two quantities obtained from the TOF of the observed peaks are the phonon frequency and from the scattering angle the parallel momentum component of the phonon. The resolution of these two are limited by the velocity and angular resolution to approximately 3% and 1%, respectively.^{2,3} For angular scans the chopper was moved out of the path of the beam and the scattered signal was measured as a function of the incident angle by rotating the crystal. The relative angular setting was accurate to 0.01° , the absolute to 0.2° .

III. RESULTS

A. TOF spectra

Some representative TOF spectra near $\theta_i = 60^\circ$ are shown in Fig. 2. As we shall see below, this angular region is interesting because of the large region of overlap with the dispersion curves. Since the intensity scale has been normalized (see preceding section) the relative intensities in the six runs can be compared directly. The triangles at the bottom of each spectrum indicate the expected locations of elastic scattering. As observed in the previous work on LiF, NaF, and KCl, elastic scattering from crystal imperfections produces a small contribution which is largest near the diffraction peak at $\theta_i \simeq 60^\circ$. At angles removed by 1.5° , as at $\theta_i = 61.8^\circ$, this spurious signal has virtually disappeared. The large elastic peak at $\theta_i = 59.0^\circ$ appears to be anomalous. As will be discussed, most but not all of the other structures seen in the spectra can be attributed to phonons.

The sharp single peaks in the TOF spectra indicate that the inelastic collisions are dominated by single-phonon processes. The equations of conservation of energy and momentum for single-phonon inelastic scattering are

$$k_f^2 = k_i^2 + 2m\omega/\hbar, \quad (1)$$

$$\Delta \vec{K} = \vec{K}_f - \vec{K}_i = \vec{G}_{mn} + \vec{Q}, \quad (2)$$

where m is the mass of He and ω is the frequency of the

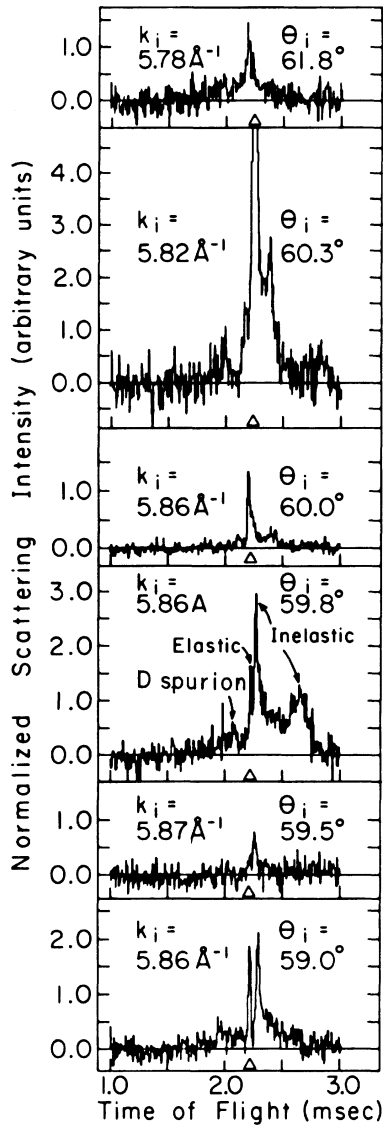


FIG. 2. Normalized measured TOF spectra for He-NaCl(100) for various incident angles near 60° . The $(\bar{1}\bar{1})$ diffraction peak is at 60° . The structure interpretation is shown on the curve for $\theta_i = 59.8^\circ$. The triangle marks the location of the elastic TOF, while the structure on either side is from inelastic scattering or "D spurions."

surface phonon with momentum \vec{Q} ; $\omega > 0$ denotes annihilation and $\omega < 0$ denotes creation of a surface phonon. The capital letters \vec{K}_f , \vec{K}_i , and \vec{G}_{mn} refer to surface components of the scattered and incident wave vectors and the reciprocal-lattice vector of order mn , respectively. $\vec{G}_{mn} = \vec{Q} = 0$ describes elastic specular scattering; if $\vec{Q} = 0$, $\vec{G}_{mn} \neq 0$ diffraction takes place, and if $\vec{Q} \neq 0$, inelastic scattering occurs. $\vec{Q} > 0$ and $\vec{Q} < 0$ correspond to forward and backward inelastic scattering, respectively.

For planar scattering along a surface-symmetry direction the one-phonon inelastic events involve exclusively phonons with momentum \vec{Q} in the scattering plane. Under these conditions the conservation equation can be rewritten as

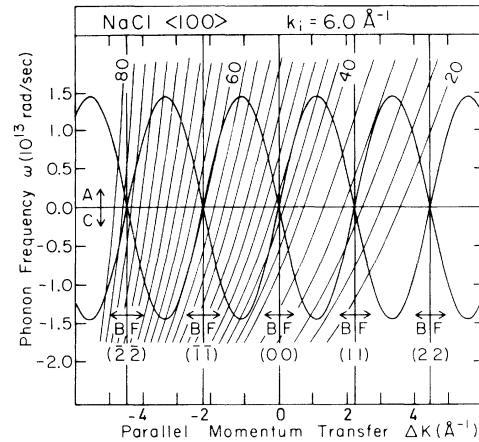


FIG. 3. Extended zone plot of dispersion curves and scan curves for NaCl. The dispersion curves (dark solid lines) are the Rayleigh dispersion waves in the sine approximation and the scan curves (labeled by incident angle θ_i) are from the solution of Eq. (4) for $k_i = 6 \text{ \AA}^{-1}$. $\Delta K = -2.23 \text{ \AA}^{-1}$, $+2.23 \text{ \AA}^{-1}$ and 0 corresponds to $(\bar{1}\bar{1})$, (11) diffraction and specular scattering, respectively. The positive and/or negative values of ω refer to phonon annihilation and/or creation, respectively, and they are labeled A and C. The F, B refers to phonons directed forward and backward with respect to K_i . The work reported here was generally at $k_i = 5.85$ or 6.1 \AA^{-1} so the scan curves at $k_i = 6.0 \text{ \AA}^{-1}$ are only approximate for the above two wave vectors.

$$Q = k_i \cos \theta_i \left[\frac{\hbar \omega}{E_i} + 1 \right]^{1/2} - (K_i + G_{mn}) \quad (3)$$

or

$$\frac{\hbar \omega}{E_i} = \frac{(K_i + G_{mn} + Q)^2}{k_i^2 \cos^2 \theta_i} - 1, \quad (4)$$

where E_i is the incident energy. We use Eq. (3) with the observed energy loss associated with the time difference between the elastic and inelastic peaks in the TOF spectra to calculate the phonon momentum for that inelastic peak. In Eq. (4) we have a relationship between all possible phonon frequencies ω and the total momentum transfer $\Delta K = Q + G_{mn}$ consistent with the conservation equations. Figure 3 is a plot of such a relation (scan curve) with $k_i = 6 \text{ \AA}^{-1}$ for various values of θ . Also shown is an extended Rayleigh-wave dispersion curve. The intersections of the scan curves with the dispersion curves indicate the possible solutions of the conservation equations where maxima might be observed in the TOF spectra due to inelastic collisions with phonons. Of course an interaction with bulk phonons and other surface localized modes is possible and these may also show up as structure in the TOF spectra at the corresponding energies.

Equation (3) has been used with 33 measured TOF spectra to obtain the experimental points in Fig. 4. Note that around the (11) and $(\bar{1}\bar{1})$ reciprocal-lattice region some of the data are marked by squares and are connected by a dashed line. These peaks have been attributed to diffraction of He atoms with velocities which lie in the wings of the velocity distribution.^{2,3,28} Even though the wing in-

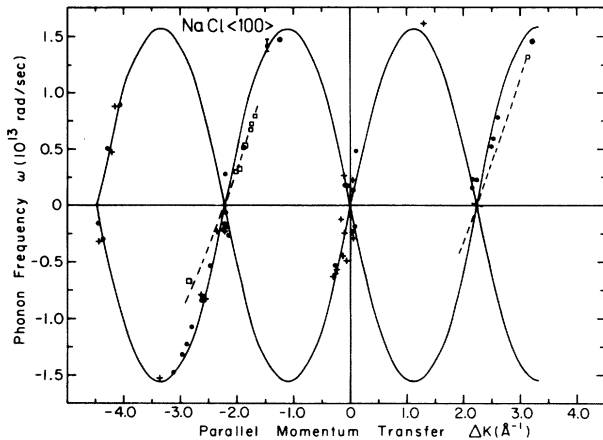


FIG. 4. Extended zone plot of measured surface-phonon frequencies and parallel momentum for the (001) surface and the $\langle 100 \rangle$ direction of NaCl. The solid curves are the surface dispersion curves for NaCl as obtained by Chen, de Wette, and Alldredge (Ref. 16). The closed circles (crosses) are obtained from inelastic events in the TOF spectra with the target at 300 K (220 K). The open squares, taken also from TOF spectra, represent the D spurions and carry no surface dispersion information (see text). A representative error bar is shown.

intensities may be 10^{-3} below that of the peak of the velocity distribution, the apparatus acts as a crystal monochromator to pick out this component, which has an intensity comparable to the inelastic intensity. These points have been previously called " D spurions".³ A simple theory allows the points to be identified and excluded from the dispersion curve since they provide no surface-phonon information.^{2,3} The other measured points cover the entire region of momentum space from $\Delta K = -4.5$ to 3.3 \AA^{-1} . It is gratifying to see that a number of points are in the region of the Brillouin-zone boundary. This is seen more clearly in Fig. 5 which shows the reduced zone plot for He scattered from NaCl with the D spurion information removed. The data is compared with the available theoretical calculations of Chen *et al.*¹⁶ as well as Benedek and Miglio.¹⁴

Some of the scatter of the data at the lowest phonon frequencies is probably due to additional interactions with the surface components of bulk modes. This is substantiated by the general agreement between the location of these points and the location of the bulk-phonon dispersion curves as taken from the speed of sound in the bulk.²⁹ Calculations of surface-projected phonon densities indicate an enhancement only at the edge of the longitudinal acoustic band but peaks due to bound-state inelastic resonances are also possible.

B. Angular distributions

The beam intensity was measured as a function of incident angle θ_i for He atoms scattering from the (001) surface of the NaCl crystal in the $\langle 100 \rangle$ direction. The incident wave vector k_i varied from 5.8 to 6.3 \AA^{-1} and the target temperature was usually maintained at 298 K, or near 220 K.

Figure 6 shows two typical angular distributions for He

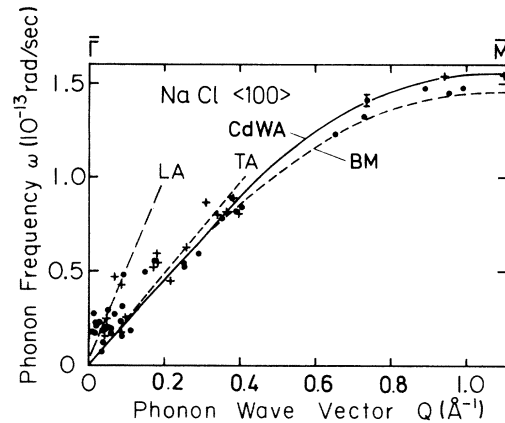


FIG. 5. Reduced zone plot for NaCl $\langle 100 \rangle$ without the D spurions points. The theoretical curve with a solid line is that of Chen, de Wette, and Alldredge (Ref. 16) and the dashed curve is from Benedek and Miglio (Ref. 14). The closed circles were taken at a surface temperature of 300 K and the crosses at 220 K. Within the error of this experiment there is no difference between these two experimental results. The bulk surface slopes of the longitudinal and transverse waves are also shown. A representative error bar is shown.

on NaCl at different k_i and target temperatures. The incident wave vector has been determined both by TOF and from the angular distribution by use of Bragg's law for diffraction; the two values agree within 1%. Further, the elastic velocity from the TOF and the experimental incident angle predict a surface lattice spacing which agrees with the bulk lattice distance of 5.640 \AA to within about 0.5%. As we shall see, the angular distributions contain a wealth of information about important features of the potential-energy curve of the He-NaCl(001) interaction as well as additional information on the surface-phonon dispersion curve. Tables I and II contain a tabulation of the experimental angles of the maxima and minima observed in the two scans of Fig. 6 as well as the interpretation (discussed below) of this structure.

1. Information on the corrugation of the atom-surface potential

The ratios of diffraction-peak intensities to specular intensity provide information on the corrugation of the periodic part of the atom-surface potential.^{8,30-32} Because of the 90° angle between ingoing and outgoing beams we expect the ratios for \vec{G} and $-\vec{G}$ to be identical. However, experience has taught us that very slight misalignments of the crystal tilt angle can cause differences in the intensities. Thus to first approximation we can correct for this by taking the average value of the ratio $I(1,1)/I(0,0)$ and $I(\bar{1},\bar{1})/I(0,0)$. The ratio from different measurements of the areas under the peaks with target at 300 K and incident wave vector $k_i = 5.85 \text{ \AA}^{-1}$ is then given by

$$\frac{I(1,1)}{I(0,0)} = \frac{I(1,1) + I(\bar{1},\bar{1})}{2I(0,0)}$$

The result obtained from six different angular scans is 128 ± 49 , where the error is the mean-square deviation.

TABLE I. Summary of the angles in Fig. 6(a) where structures are seen and the interpretation of these structures are in terms of KF and selective desorption (SD). The beam was in the $\langle 100 \rangle$ direction and the NaCl target was the (001) surface at 298 K with $k_i = 5.86 \text{ \AA}^{-1}$ and $E_i = 17.9 \text{ meV}$. The $(\epsilon_v)_{\text{calc}}$ were first calculated from a Morse potential (see text) and then Eq. (6) was used to calculate $(\theta_i)_{\text{MP}}$ which served to identify the experimental incident angles for the G_{11} or G_{10} terms. With this identification the experimental energy levels $(\epsilon_v)_{\text{expt}}$ were obtained from the structure in Fig. 6(a) and the levels were then averaged for all the angular distributions (Table III) and used to obtain the $(\theta_i)_{\text{calc}}$ angles for all of the G_{mn} terms.

| θ_i (deg) ^a Experimental | $(\theta_i)_{\text{MP}}$ (deg) Morse potential | θ_i (deg) | | G_{mn} <i>m n</i> | Bound state | $-\epsilon_v$ (meV) | | Mechanism ^b |
|---|---|--------------------------|--|------------------------|----------------|---------------------|------------|------------------------|
| | | Calculated avg values | | | | Experimental | Calculated | |
| <u>32.2</u> | | 31.9 ^c | | | | | | KF |
| <u>33.8</u> | | | | | | | | not determined |
| <u>39.</u> | 38.9 | 39.1 | | 1 1 | 3 | 0.42 | 0.355 | SD |
| <u>42.8</u> | | 41.8 ^c | | | | | | KF |
| | 46.7 | 45.9 ^d | | 1 1 | 1 | 3.7 ^e | 4.14 | SD |
| <u>46.8</u> | | 46.3 ^c | | | | | | KF |
| <u>53.3</u> | 54.3 | 53.5 | | 1 1 | 0 | 7.16 | 7.59 | SD |
| <u>56.9</u> | 57.0 | 56.8 | | 1 0 | 2 | 1.69 | 1.73 | SD |
| <u>59.4</u> | | 59.9 ^c | | | | | | KF |
| <u>64.7</u> | | 63.1 | | 1 0 | 1 | | | SD |

^aThese angles were taken from Fig. 6(a). Angles corresponding to maxima are underlined.

^bAbbreviation SD means selective desorption in which an atom is trapped into a bound state by elastic selective adsorption and then released after an interaction with a phonon. The symbol KF means kinematical focusing.

^cAngle corresponding to KF as obtained from the tangent angle of the scan curve with the dispersion curve.

^dThis predicted resonance is probably hidden by the KF peak.

^eSee Refs. 8 and 21.

TABLE II. Summary of the angles in Fig. 6(b) where structures are seen and the interpretation of those structures in terms of KF and SD. The beam was in the $\langle 100 \rangle$ direction and the NaCl crystal was the (001) surface at 220 K with $k_i = 6.1 \text{ \AA}^{-1}$ and $E_i = 19.44 \text{ meV}$. The $(\epsilon_v)_{\text{calc}}$ values were first calculated from a Morse potential (see text) and then Eq. (6) was used to calculate $(\theta_i)_{\text{MP}}$. This served to identify the experimental incident angles for G_{11} and G_{10} . With this identification the experimental energy levels $(\epsilon_v)_{\text{expt}}$ were obtained from the experimental structure of Fig. 6(b) and the levels were then averaged for all the angular distributions (Table III) and used to obtain the $(\theta_i)_{\text{calc}}$ angles for all of the G_{mn} terms.

| θ_i (deg) ^a Experimental | $(\theta_i)_{\text{MP}}$ (deg) Morse potential | θ_i (deg) | | G_{mn} <i>m n</i> | Bound state <i>v</i> | $-\epsilon_v$ (meV) | | Mechanism ^b |
|---|---|--------------------------|--|------------------------|----------------------------|---------------------|------------|------------------------|
| | | Calculated avg values | | | | Experimental | Calculated | |
| <u>16.2</u> | | 16.3 | | 2 2 | 3 | | | SD |
| <u>17.5</u> | | 18.1 | | 2 2 | 2 | | | SD |
| 28 | | | | | | | | not determined |
| <u>32.6</u> | | 32.2 ^c | | | | | | KF |
| <u>33.4</u> | | | | | | | | not determined |
| <u>40.0</u> | 40.0 | 40.2 | | 1 1 | 3 | 0.347 | 0.355 | SD |
| <u>41.5</u> | | (42.5) ^d | | 1 1 | 2 | | | SD |
| <u>43.1</u> | | 42.5 ^c | | | | | | KF |
| | 47.3 | 46.5 | | 1 1 | 1 | 3.7 ^e | 4.14 | SD |
| 47 | | 46.1 ^c | | | | | | KF |
| <u>54</u> | 54.4 | 53.7 | | 1 1 | 0 | 7.4 | 7.59 | SD |
| 57.1 | 57.6 | 57.4 | | 1 0 | 2 | 1.54 | 1.73 | SD |
| 58.9 | | 59.5 ^c | | | | | | KF |
| 64 | | 63.3 | | 1 0 | 1 | | | SD |

^aThese angles were taken from Fig. 6(b). Angles corresponding to maxima are underlined.

^bAbbreviation SD means selective desorption, in which an atom is trapped into a bound state by elastic selective adsorption and then released after an interaction with a phonon. The symbol KF means kinematical focusing.

^cStructure is caused by KF and the angle is obtained from the tangent angle of the scan curve with the dispersion curve.

^dThis result is listed as uncertain because KF and the listed resonance are close together.

^eSee Refs. 8 and 21.

The He-NaCl corrugation is greater than that for LiF ($\zeta_0=0.31 \text{ \AA}$),⁹ which is expected according to the rigid-ion model.¹⁹ We point out, however, that in view of the very good energy resolution the ratio of the intensities may be rather severely affected by resonance effects. Recent theoretical and experimental work³³ on He-LiF shows that particularly in the energy region of these experiments bound-state resonances can considerably modify both the (00) and the first-order diffraction intensities in different directions depending on the exact value of k_i . Unfortunately, a close-coupling calculation is only possible for a soft repulsive potential and at present not enough data is available for He-NaCl to justify such a calculation.

2. Bound states

The conditions for elastic selective adsorption with phonon-assisted desorption (called selective desorption) are obtained by assuming the crystal has an attractive potential well with vibrational bound states ϵ_v ($\epsilon_v < 0$). The condition for elastic selective adsorption is then⁸

$$k_z^2 = k_i^2 - (K_i + G_{mn})^2 = -(2m/\hbar^2) |\epsilon_v|, \quad (6)$$

where k_z is the z component of the wave vector and all of the other terms have previously been defined. We use the Morse-model potential for He-NaCl with well depth $D = -9.7 \text{ meV}$ as recommended by Hoinkes⁸ and a reciprocal range parameter $\kappa = 1.0 \text{ \AA}^{-1}$ to obtain initial trial bound-state energies. They are listed as $(\epsilon_v)_{\text{calc}}$ in Tables I and II. These bound-state energies were used with $E_i = 17.88 \text{ meV}$, $k_i = 5.86 \text{ \AA}^{-1}$, and also $E_i = 19.41 \text{ meV}$, $k_i = 6.1 \text{ \AA}^{-1}$, and Eq. (6) above to obtain the $(\theta_i)_{\text{MP}}$ terms, where MP is the Morse potential, for G_{11} in Tables I and II, respectively. The calculations suggest that the $(\theta_i)_{\text{expt}} = 39^\circ$ and 53.3° maxima in Table I and the $(\theta_i)_{\text{expt}} = 40^\circ$ and 54° maxima in Table II are associated with G_{11} and are due to selective desorption via the $v=3$ and 0 bound states, respectively. The $G_{11}, v=2$ term is predicted to lie near or under the $\theta_i = 43^\circ$ KF peak (discussed later) which cannot therefore be observed. Thus there is no evidence for this energy level, although there is a peak at 41.5° in Fig. 6(b) which may be the $v=2, G_{11}$ level. The Morse potential does predict an extremum for $v=2$ and the G_{10} reciprocal wave vector which is very near an experimental minimum, which occurs in both Figs. 6(a) and 6(b). This angle is used for ϵ_2 and the experimental energy for it is listed in Tables I and II. The $G_{11}, v=1$ term is predicted to be under the KF peak so that it cannot be easily obtained from this work. We use

TABLE III. Average values of the bound-state energies for the He-NaCl system taken from up to ten different angular distribution measurements. The uncertainty is that represented in the scatter in the measurements.

| State | $-\epsilon_v \pm \Delta\epsilon_v$ (meV) |
|----------------|--|
| 0 | 7.21 ± 0.10 |
| 1 ^a | 3.7 |
| 2 | 1.62 ± 0.07 |
| 3 | 0.41 ± 0.12 |

^aTaken from Refs. 8 and 21.

instead the previously measured value²¹ $\epsilon_1 = -3.7 \text{ meV}$ to predict $(\theta_i)_{\text{calc}} = 45.9^\circ$ and 46.5° for G_{11} of Tables I and II, respectively. This level is consistent with our results.

Following the above procedure we have taken the average from up to ten of our distributions to provide the three energy levels listed in Table III. These are then used in the calculation of the angles $(\theta_i)_{\text{calc}}$ in Tables I and II which are also plotted in Fig. 6. Between the selective adsorption features at these angles and the KF features discussed in Sec. III B 3 nearly all of the structures in Tables I and II can be assigned in a consistent fashion.

3. KF and determination of surface-phonon dispersion curves

The scan curves of Fig. 3 have a tangent contact with the dispersion curves at approximate angles of $\theta_i = 8^\circ, 16^\circ, 25.5^\circ, 32^\circ, 42.5^\circ, 46^\circ,$ and 60° . At these angles an increase

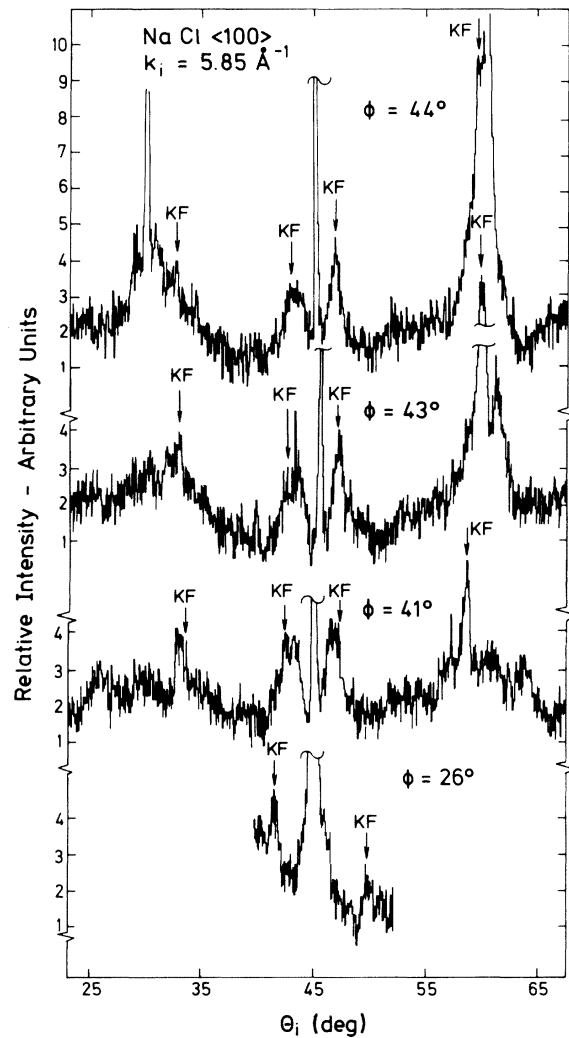


FIG. 7. Angular distribution for the scattered He intensity as a function of incident angle for He-NaCl at different azimuthal angles ϕ . Curves A–D have azimuthal angles of $44^\circ, 43^\circ, 41^\circ,$ and 26° , respectively (45° is the $\langle 100 \rangle$ direction). These should be compared to Fig. 6(a). Note that the diffraction and resonance structure decreases dramatically and only the KF enhancements remain. These are shown by arrows.

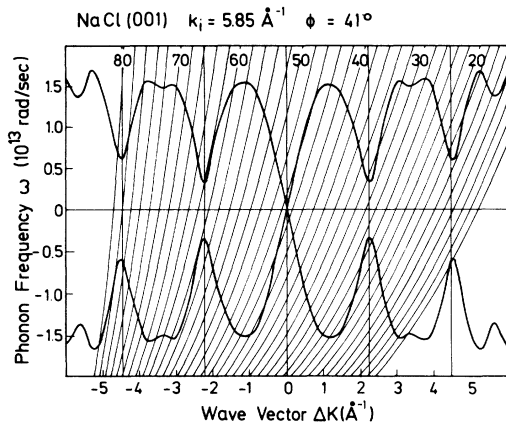


FIG. 8. Plot of the theoretical dispersion curves ω vs ΔK for NaCl for an azimuthal angle $\phi = 41^\circ$ ($\phi = 45^\circ$ is the $\langle 100 \rangle$ direction). The scan curves, as a function of incident angle, locate the position of the tangent points for KF. The incident wave vector is 5.85 \AA^{-1} .

in intensity of the scattered beam has been theoretically predicted by one of us³⁴ and termed KF. The KF behavior has been clearly observed in the He-NaF interaction and the methods for identifying KF structures are discussed elsewhere.³⁵

On one side of the KF angle the scan intersects the dispersion curve twice and on this side the intensity increases approximately as $|\theta_i - \hat{\theta}_i|^{-1/2}$ as θ_i approaches the KF angle $\hat{\theta}_i$. Beyond this angle the intensity is expected to fall off abruptly. We call these the bright and dark sides of the KF singularity, respectively. This means that at or near the above angles $\hat{\theta}_i$ we should see maxima in intensity in the angular distributions. KF will also affect the TOF spectra. As we approach $\hat{\theta}_i$ from the bright side the corresponding TOF peaks will coalesce and disappear suddenly as the angle passes over to the dark side.

A suitable region in the TOF spectra for seeing such an effect in creation is near 60° as is shown in Figs. 2 and 3. If we start in Fig. 2 with the TOF spectra for $\theta_i = 59^\circ$ we find intensity only from the creation forward dispersion curve as well as some from bulk bands. The amplitudes are even smaller at $\theta_i = 59.5^\circ$, but at $\theta_i = 59.8^\circ \approx \hat{\theta}_i$ a large increase in intensity is seen as well as the new peak from creation backward scattering. This is a clear indication of KF. The intensity drops off sharply as θ_i increases and the KF from the annihilation part of the dispersion curve

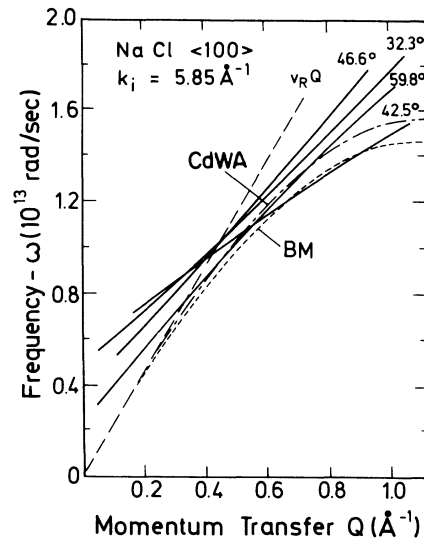


FIG. 9. Summary of the scan curves for the KF incident angles of Table IV. Included is the dashed straight line representing the Rayleigh-wave dispersion in the continuum limit. These curves envelope the dispersion curve and represent another method of obtaining dispersion-curve information. Dotted and dot-dashed curves are from the calculations of Benedek and Miglio (BM) (Ref. 14) and Chen, de Wette, and Alldredge (Ref. 16), respectively.

is hidden by the diffraction peak as well as by the condition that the tangent contact has different curvature on the annihilation side as compared to the creation side.

For the other angular regions where KF might be expected, we do not have sufficient TOF spectra to clearly determine if this is the case. The spectra at angles slightly below and above $\theta_i = 45^\circ$ as well as the spectra near $\theta_i = 32^\circ$ are, however, consistent with KF. TOF spectra were not measured at the other listed angles. A further simpler check on whether or not a given maximum is due to KF can be made by measuring angular distributions for different values of the azimuthal angle. Under these conditions both the diffraction peaks and the predominantly in-plane resonances disappear. KF structures, however, are expected to remain and change in predictable ways.³⁵

Figure 7 shows the angular distributions corresponding to Fig. 6(a) for azimuthal angles $\phi = 44^\circ, 43^\circ, 41^\circ$, and 26° ($\phi = 45^\circ$ is the $\langle 100 \rangle$ direction). Here the diffraction peaks and small-resonance structures are substantially reduced or no longer seen and only the KF contribution to

TABLE IV. Summary of measured KF angles in NaCl as a function of ϕ for incident wave vector $k_i \approx 5.85 \text{ \AA}^{-1}$.

| ϕ (deg) Azimuthal angle | Shape of KF resonance and angle (deg) | | | |
|------------------------------------|---|---|--|---|
| |  |  |  |  |
| 45 | 32.2 | 42.8 | 46.8 | 60.0 |
| 44 | 32.1 | 42.6 | 46.0 | 60.5 |
| 43 | 32.2 | 42.5 | 46.4 | 59.5 |
| 41 | 32.9 | 42.2 | 47.4 | 59.2 |
| Average value | 32.3 ± 0.4 | 42.5 ± 0.3 | 46.6 ± 0.6 | 59.8 ± 0.6 |

the intensity appears to cause structures. That this is the most reasonable interpretation is shown in Fig. 8 where the cuts through the estimated three-dimensional Rayleigh-mode dispersion surfaces corresponding to $\phi=41^\circ$ are shown along with the scan curves. It is interesting to note that the dispersion curves near the specular peak are affected least, whereas the effect increases with increasing ΔK . Thus the KF maxima near the specular should remain largely unaffected as we rotate the crystal as observed in Fig. 8.

Table IV contains a summary of the measured incident angles corresponding to tangency points for several values of ϕ at and near 45° where measurements were made. In this limited range of ϕ and measured peaks we would expect the measured incident angles to change only slightly as is observed. For this reason also we have reported the average values for all four measurements and use these values as the KF angles for $\phi=0$.

By assuming interactions only with Rayleigh phonons these KF angles contain information on the dispersion curves. This is shown in Fig. 9 where the tangent sections of the scan curves corresponding to the average value of the angles of Table IV are plotted. The curve for the long-wavelength limit is obtained from the surface-phonon velocity in the long-wavelength limit.²⁹ The assignment of the peaks in the angular distributions due to KF are also listed in Tables I and II.

IV. CONCLUSIONS

The measured dynamical information for the Rayleigh dispersion curve for NaCl shows satisfactory agreement with theoretical calculations for an unrelaxed surface. The experimental points lie between the results from slab dynamics of Chen, de Wette, and Alldredge based on the shell model¹⁶ and the Green's-function approach used by

Benedek and Miglio and based on the breathing-shell model.¹⁴ At the zone boundary they appear to lie somewhat closer to the former calculations. From the agreement between experiment and the theoretical calculations where surface elastic relaxation and the surface change of electronic polarizability have been neglected, we must conclude that either these effects are weak or that they compensate each other.^{6,13-15} Thus the present data does not provide any new information on the effect of the surface discontinuity on the forces between the ions of an ionic crystal.

A very interesting feature of this work was the observation of structure in the angular distributions corresponding to KF. In this paper we were able to identify these structures by out-of-plane angular scans. Once identified we were able to use the scan curves corresponding to KF to outline the dispersion curve. This new method offers a rapid way to explore the dynamics of crystal surfaces. Simply by adjusting k_i and θ_i the necessary information can be directly obtained. It is particularly useful to have KF occur near the edge of the surface Brillouin zone for this gives direct information on the dispersion behavior there.

ACKNOWLEDGMENTS

We thank H. Hoinkes for sending us a copy of the Ph.D. thesis of J. R. Bledsoe and for helpful comments on NaCl crystals. We wish to thank D. Eichenauer for calculating the position of resonance structure in this system. Two of us (J.G.S.) and (G.B.) are thankful to the Max-Planck-Institut für Strömungsforschung, for making their visits to Göttingen possible. R. B. Doak thanks the Deutsche Forschungsgemeinschaft (Sonderforschungsbereich 126 at the University of Göttingen) for providing financial support.

*Permanent address: Gruppo Nazionale di Struttura della Materia del Consiglio Nazionale delle Ricerche, Dipartimento di Fisica dell'Università degli Studi di Milano, I-20133 Milano, Italy.

†Present address: Bell Laboratory, 600 Mountain Ave., Murray Hill, New Jersey 07974.

‡Permanent address: Department of Physics, The Florida State University, Tallahassee, Florida 32306.

¹G. Brusdeylins, R. B. Doak, and J. P. Toennies, *Phys. Rev. Lett.* **44**, 1417 (1980); **46**, 437 (1981).

²R. B. Doak, Ph.D. thesis, Massachusetts Institute of Technology, Cambridge, Massachusetts, 1981 (unpublished); Bericht 4/1981 Max-Planck-Institut für Strömungsforschung.

³G. Brusdeylins, R. B. Doak, and J. P. Toennies, *Phys. Rev. B* **27**, 3662 (1983).

⁴J. P. Toennies, in *Dynamics of Gas-surface Interaction*, edited by G. Benedek and U. Valbusa (Springer, Berlin, 1982).

⁵R. B. Doak and J. P. Toennies, *Surf. Sci.* **117**, 1 (1982).

⁶G. Benedek, G. Brusdeylins, R. B. Doak, and J. P. Toennies, *J. Phys. (Paris) Colloq.* **42**, C6-793 (1981).

⁷G. Brusdeylins, R. B. Doak, and J. P. Toennies, *J. Chem. Phys.* **75**, 1784 (1981).

⁸H. Hoinkes, *Rev. Mod. Phys.* **52**, 933 (1980).

⁹T. Engel and K. H. Rieder, *Structural Studies of Surfaces*, Vol. 91 of *Springer Tracts in Modern Physics*, edited by G. Höhler (Springer, Berlin, 1982), pp. 55-180.

¹⁰G. Brusdeylins, R. B. Doak, J. G. Skofronick, and J. P. Toennies *Surf. Sci.* **128**, 191 (1983).

¹¹G. Lilienkamp and J. P. Toennies, *Phys. Rev. B* **26**, 4752 (1982).

¹²G. Lilienkamp and J. P. Toennies, *J. Chem. Phys.* **78**, 5210 (1983).

¹³J. P. Toennies, *Phys. Scr.* **T1**, 89 (1982).

¹⁴G. Benedek and L. Miglio, in *Ab Initio Calculation of Phonon Spectra*, edited by J. T. Devreese, V. E. van Doren, and P. E. von Camp (Plenum, New York, 1982), p. 215.

¹⁵G. Benedek, G. P. Brivio, L. Miglio, and V. R. Velasco, *Phys. Rev. B* **26**, 497 (1982).

¹⁶T. S. Chen, F. W. de Wette, and G. P. Alldredge, *Phys. Rev. B* **15**, 1167 (1977).

¹⁷G. Benedek, *Surf. Sci.* **61**, 603 (1976).

¹⁸J. R. Bledsoe and S. S. Fisher, *Surf. Sci.* **46**, 129 (1974); *J. Vac. Sci. Technol.* **9**, 819 (1972).

¹⁹K. H. Rieder, *Surf. Sci.* **118**, 57 (1982).

²⁰N. Garcia, G. Armand, and J. Lapujoulade, *Surf. Sci.* **68**, 399 (1977).

²¹J. R. Bledsoe, Research Laboratories for the Engineering Sciences, University of Virginia, Report No. AEEP-3719-101-72U (unpublished).

²²S. Iannotta and U. Valbusa, *Surf. Sci.* **100**, 28 (1980).

²³L. Bätz, H. Hoinkes, and H. Wilsch, *Surf. Sci.* **120**, L417 (1982).

- ²⁴J. P. Toennies and K. Winkelmann, *J. Chem. Phys.* **66**, 396 (1977).
- ²⁵G. Brusdeylins, H.-D. Meyer, J. P. Toennies, and K. Winkelmann, in *Progress in Astronautics and Aeronautics 5*, edited by J. L. Potter (American Institute of Aeronautics and Astronautics, New York, 1977), p. 1047.
- ²⁶Dr. Karl Korth, Monokristalle—Offene Handels Gesellschaft (OHG), Am Jägersberg 9, D-2300 Kiel 17, Federal Republic of Germany.
- ²⁷J. Estel, H. Hoinkes, H. Kaarmann, H. Nahr, and H. Wilsch, *Surf. Sci.* **54**, 393 (1976).
- ²⁸W. Allison, R. W. Willis, and M. Cardillo, *Phys. Rev. B* **23**, 6824 (1981).
- ²⁹Calculated from bulk constants. See G. W. Farnell in *Physical Acoustics*, edited by W. P. Mason and R. N. Thurston VI (Academic, New York, 1970), pp. 109–166.
- ³⁰U. Garibaldi, A. C. Levi, R. Spadacini, and G. E. Tommei, *Surf. Sci.* **48**, 649 (1975).
- ³¹G. Boato, P. Cantini, and L. Mattera, *Surf. Sci.* **55**, 141 (1976).
- ³²C. Chiroli and A. C. Levi, *Surf. Sci.* **59**, 325 (1976).
- ³³G. Drolshagen, A. Kaufhold, and J. P. Toennies, *Isr. J. Chem.*, **22**, 283 (1982).
- ³⁴G. Benedek, *Phys. Rev. Lett.* **35**, 234 (1975).
- ³⁵G. Benedek, G. Brusdeylins, R. B. Doak, and J. P. Toennies, *Phys. Rev. B* **27**, 2488 (1983).